The unfolded protein response: a novel therapeutic target for poor prognostic BRAF mutant colorectal cancer

Forsythe, N., Refaat, A., Javadi, A., Khawaja, H., Weir, J-A., Emam, H., ... Van Schaeybroeck, S. (2018). The unfolded protein response: a novel therapeutic target for poor prognostic BRAF mutant colorectal cancer. Molecular Cancer Therapeutics. DOI: 10.1158/1535-7163.MCT-17-0603

Published in:
Molecular Cancer Therapeutics

Document Version:
Early version, also known as pre-print

The unfolded protein response: a novel therapeutic target for poor prognostic *BRAF* mutant colorectal cancer

Nicholas Forsythe[1,‡], Alaa Refaat[1,‡], Arman Javadi[1], Hajrah Khawaja[1], Jessica-Anne Weir[1], Heba Emam[1], Wendy L. Allen[1], Frank Burkamp[2], Vlad Popovici[3], Puthen V. Jithesh[4], Claudio Isella[5,6], Melissa J. Labonte[1], Ian G. Mills[1], Patrick G. Johnston[1,†], Sandra Van Schaeybroeck[1,*]

[1]Drug Resistance Group, Centre for Cancer Research and Cell Biology, School of Medicine, Dentistry and Biomedical Science, Queen's University Belfast, 97 Lisburn Road, Belfast, BT9 7AE, United Kingdom.

[2]Almac Discovery Laboratories, Centre for Precision Therapeutics, 97 Lisburn Road, Belfast, BT9 7AE, United Kingdom.

[3]Research Centre for Toxic Compounds in the Environment, Faculty of Science, Masarykova Univerzita, Kamenice 5, 625 00 Brno, Czech Republic.

[4]Division of Biomedical Informatics, Sidra Medical and Research Center, PO Box 26999, Education City North Campus, Doha, Qatar.

[5]Department of Oncology, University of Torino School of Medicine, 10060 Candiolo Torino, Italy.

[6]Candiolo Cancer Institute-FPO IRCCS, 10060 Candiolo Torino, Italy.

[‡] Equal contribution

[†] Deceased

Running title: UPR, novel target in poor prognostic *BRAF*MT colon cancer

Keywords: Oncogenic *BRAF*, UPR, ER stress, apoptosis, colorectal cancer

[*]To whom correspondence should be addressed, at the Centre for Cancer Research and Cell Biology, Queen's University Belfast, 97 Lisburn Road, Belfast BT9 7AE, Northern Ireland. Tel: 44-2890-972954. Fax: 44-2890-972776. Email: s.vanschaeybroeck@qub.ac.uk

Financial support: Funding was supported by Cancer Research UK (C212/A13721 – P.G. Johnston); Cancer Research UK fellowship (C13749/A13172 – S. Van Schaeybroeck) and by MErCuRIC, funded by the European Commission's Framework Programme 7, under contract #602901 (S. Van Schaeybroeck).

Conflicts of interest: P.G. Johnston was the founder and held shares in Almac diagnostics, Fusion Antibodies and CV6 Therapeutics and acted as an advisor/consultant to Pfizer and Chugai Pharmaceuticals. The other authors declare no competing interests.

ABSTRACT

BRAF^{V600E} mutations occur in ~10% of colorectal cancer (CRC) cases, are associated with poor survival and have limited responses to BRAF/MEK inhibition with or without EGFR inhibition. There is an unmet need to understand the biology of poor prognostic *BRAF*MT CRC. We have used differential gene expression and pathway analyses of untreated stage II and stage III *BRAF*MT (discovery set: n=31; validation set: n=26) CRC and an siRNA screen to characterize the biology underpinning the *BRAF*MT subgroup with poorest outcome. These analyses identified the unfolded protein response (UPR) as a novel and druggable pathway associated with the *BRAF*MT CRC subgroup with poorest outcome. We also found that oncogenic *BRAF* drives endoplasmic reticulum (ER) stress and unfolded protein response (UPR) pathway activation through MEK/ERK. Furthermore, inhibition of GRP78, the master regulator of the UPR, using siRNA or small molecule inhibition, resulted in *acute* ER stress and apoptosis, in particular in *BRAF*MT CRC cells. In addition, dual targeting of protein degradation using combined Carfilzomib (proteasome inhibitor) and ACY-1215 (HDAC6-selective inhibitor) treatment resulted in marked accumulation of protein aggregates, acute ER stress, apoptosis and therapeutic efficacy in *BRAF*MT *in vitro* and xenograft models. Mechanistically, we found that the apoptosis following combined Carfilzomib/ACY-1215 treatment is mediated through increased CHOP expression. Taken together, our findings indicate that oncogenic *BRAF* induces chronic ER stress and that inducers of acute ER stress could be a novel treatment strategy for poor prognostic *BRAF*MT CRC.

INTRODUCTION

Mutations in *BRAF* at position 600 from valine (V) to glutamic acid (E) occur in ~10% of colorectal cancers (CRC). *BRAF*^{V600E} mutations, which account for more than 80% of all *BRAF* mutations (1), lead to sustained MAPK signalling and are associated with poor survival and drug resistance (2, 3). Trials investigating the effect of BRAF inhibition given as monotherapy have failed in *BRAF*MT CRC (3). The more recent trials with BRAF/EGFR double-therapy or BRAF/MEK/EGFR triple-therapy have shown some increased response rates but at the cost of increased toxicity (4, 5).

The endoplasmic reticulum (ER) is recognized as a major site for protein synthesis/folding (6). Increased protein synthesis/misfolding rates that exceed the capacity of protein chaperones contribute to the development of ER stress. ER stress is sensed by 3 upstream transmembrane proteins, Inositol-Requiring Protein-1 (IRE1), Protein kinase RNA-like ER Kinase (PERK) and Activating Transcription Factor-6 (ATF6). Under basal conditions, the ER chaperone GRP78 constitutively binds to the three sensors, thus preventing their activation. Upon induction of ER stress, sequestration of GRP78 by unfolded proteins results in activation of the ER-specific unfolded protein response (UPR), which attempts to reduce protein load on the ER and increases its folding capacity. PERK and IRE1α become activated following dimerization and auto-phosphorylation (7, 8). Dissociation of GRP78 from ATF6 results in translocation of the receptor to the Golgi where it is cleaved by SP1 and SP2 proteases into an active transcription factor (9). Unresolved ER stress can lead to apoptosis through upregulation of the pro-apoptotic transcription factor CHOP, resulting in downregulation of the anti-apoptotic protein BCL-2 and upregulation of pro-apoptotic proteins such as DR5 and the BH3-only proteins PUMA, NOXA and BIM (10-12).

In this study, we have used publicly available microarray datasets from CRC patients to identify novel pathways associated with the *BRAF*MT subgroup with the poorest outcome. RNAi, cellular and mechanistic assays and xenograft studies indicate that inducers of *acute* ER stress can be a novel treatment strategy for poor prognostic *BRAF*MT CRC.

MATERIALS AND METHODS

Materials

Carfilzomib, ACY-1215 and trametinib were purchased from SelleckChem (Suffolk, UK), AZD6244 (13) from AstraZeneca (Macclesfield, UK) and Z-VAD-FMK (14) from Calbiochem (Hertfordshire, UK). HA15 was generated in house (15). HA15 was synthesised from commercial *N*-(4-(3-aminophenyl)thiazol-2-yl)acetamide and commercial dansyl chloride, according to the literature (WO2014/072486). siRNAs targeting Caspase-8, Caspase-9, HSPA5 and CHOP were purchased from Qiagen (Crawley, UK) and Invitrogen respectively. The ON-Targetplus siRNA library was obtained from Dharmacon (Lafayette, USA). The *BRAF*V600E plasmid was a gift from Prof. Marais (London, UK)(16).

Cell culture

Authentication and culture of LIM2405, HT-29, VACO432/VT1, RKO, COLO205, COLO320 and CACO-2 CRC cells have previously been described (17, 18). All cells were passaged for a maximum of 2 months, after which new seed stocks were thawed. LIM2405 cells were a gift from Dr. Whitehead (Vanderbilt University, Nashville, TN) in 2010 (19). VACO432, VT1 and RKO were provided by Prof. Vogelstein (Johns Hopkins University School of Medicine, Baltimore) in 2012. HT-29 (2001), CACO-2 (2005), COLO205 (2012) and COLO320 (2012) cells were obtained from the American Type Culture Collection (Authentication by short tandem repeat profiling/karyotyping/isoenzyme analysis). DiFi cells were obtained from Dr. Montagut (Barcelona, Spain)(20).

Western blotting

Western blotting has previously been described (18). Anti-pEIF2α^{S51}, anti-EIF2α, anti-ATF4, anti-GRP78, anti-IRE1α, anti-acetylated-*α*-tubulin, anti-BCL2, anti-BCLXL, anti-PUMA, anti-BID, anti-BIM (Cell Signaling Technology, Beverly, MA, USA) and anti-pIRE1α^{S724} (Abcam, Cambridge) were used in conjunction with a HRP-conjugated anti-rabbit secondary antibody (Amersham, Buckinghamshire, UK). Anti-caspase-8 (12F5; Alexis, San Diego, CA, USA),

anti-CHOP (Cell Signaling Technology), anti-ATF6 (Abcam), anti-MCL1 (BD pharmingen, Oxford, UK) and anti-NOXA (Abcam) mouse monoclonal antibodies were used in conjunction with a horseradish peroxidase–conjugated anti-mouse secondary antibody (Amersham).

Flow cytometry

Apoptosis was evaluated using propidium iodide (PI) staining to determine the percentage of cells with DNA content <2N (18). For annexin/PI analysis, cells were harvested and analysed according to the manufacturer's instructions (BD Biosciences).

Caspase activity assays

Caspase-8 or caspase-3/7-GLO reagents (25μl) (Promega, Southampton, UK) were incubated with 5μg of protein lysate diluted in cell culture medium in a total volume of 50μl for 45 minutes at room temperature. Luciferase activity was measured using a luminometer.

MTT assays

Cell viability was determined using 3-(4,5-dimethylthiazol-2-yl)-2,5-diphenyltetrazolium bromide (MTT) (18).

Fluorescence microscopy to assess aggregated protein cargo

The PROTEOSTAT® Aggresome Detection Kit (Enzo Life Sciences LTD, UK) was used to detect aggregated protein cargo, according to the manufacturer's instructions. Images were obtained using the Leica SP5 confocal microscope.

Nascent protein synthesis labelling

Click-iT L-homopropargylglycine (HPG) Alexa Fluor 488 Protein Synthesis Kit (ThermoFisher Scientific) was used to label newly synthesized protein following the manufacturer's protocol. Detailed methodology can be found in the supplementary methods.

Real-time reverse transcription-PCR analysis

Q-PCR analysis was performed using the LightCycler® 480 probes master mix (LightCycler® 480II, Roche).

siRNA transfections

siRNA transfections were carried out using Hiperfect (Qiagen) as previously described (18).

Data analysis.

Generation of gene lists. Initial data analysis was carried out using the R Statistical Package (version 3.2.1). The data used in this study was obtained from 566 Affymetrix U133 Plus 2.0 CRC patient transcriptional profiles accessed through the NCBI GEO accession number GSE39582 (21) (discovery data set) and from the 359 Almac stage II CRC DSA CRC patient transcriptional profiles, available in the ArrayExpress database (E-MTAB-863/E-MTAB-864) (Fig. S1). *BRAF*V600E mutational status within GSE39582 was assessed by allelic discrimination using TaqMan probes (21). Mutational data for *BRAF* was unavailable for the Almac dataset, and we used a highly specific classifier to produce a *BRAF*MT surrogate status (Supplementary Methods). Within the untreated stage II/III GSE39582 and the stage II E-MTAB-863/E-MTAB-864 datasets, 31 and 26 patients were identified as *BRAF*MT respectively. A genelist was created of those genes that were differentially expressed between poor and good prognostic *BRAF*MT CRC subgroups, as described further in the Supplementary Methods.

Pathway Analysis. This was carried out using Ingenuity Pathway Analysis (IPA; Qiagen Bioinformatics), using the gene lists differentially expressed between poor and good prognostic *BRAF*MT CRC patients.

***In vivo* study.** *In vivo* studies were conducted as previously described using 6-8-week-old, female BALB/c nude mice (Envigo, UK) (18). In the initial tolerability study, 3 healthy mice received ACY-1215 30mg/kg/day IP (Day 1-Day 5 and Day 8-Day 12) alone or in combination with Carfilzomib 6mg/kg IP (Day 1/Day 3/Day 5/Day 8/Day 10/Day 12). In the efficacy study, ACY-1215 30mg/kg/day IP alone or with Carfilzomib 6mg/kg 3/week IP was administered to BALB/c nude mice with VACO432 tumours. Each treatment group contained 7 animals. Mice were sacrificed and tumours were excised on day 15. All animal experiments were carried out according to UKCCCR guidelines under licence PPL2704. *In vivo* experiments were carried out in accordance with the Animals (Scientific Procedures) Act, 1986, and approved by the Department of Health, Social Services and Public Safety, Northern Ireland.

Statistical analysis

Student's *t*-tests and 2-way ANOVA were calculated using the GraphPad software (Prism5). 2-way ANOVA test was used to determine the significance of change in levels of apoptosis between different treatment groups. Significant changes had p-values <0.05 (* $p<0.05$; ** $p<0.01$; *** $p<0.001$; ns not significant). The nature of the interaction between carfilzomib and ACY-1215 was determined using the method of Chou and Talalay (18).

RESULTS

Pathway analysis of genelists underpinning poor prognostic *BRAF*MT CRC. In order to identify novel pathways associated with the *BRAF*MT CRC subgroup with the poorest outcome, we generated differentially expressed gene lists between poor and good prognostic stage II/III *BRAF*MT CRC tumours, using the publicly available transcriptionally profiled GSE39582 CRC dataset (1.3-fold cut-off; $p < 0.05$) (Fig. S1)(21). To identify pathways that are deregulated in poor prognostic *BRAF*MT CRC, pathway analyses were carried out using both the significantly up-regulated and down-regulated genes in the poor prognostic *BRAF*MT subgroup compared to the good prognostic *BRAF*MT subgroup (Table S1 and Table S2). These results showed that cholesterol biosynthesis, the geranylgeranyldiphosphate biosynthesis and mevalonate pathway, G-protein coupled receptor signalling and the unfolded protein response (UPR), were the top 5 pathways identified from the significantly upregulated gene list in poor prognostic *BRAF*MT CRC (Table S1).

We also identified the UPR as a pathway associated with the *BRAF*MT subgroup with poor outcome, using a second untreated stage II CRC dataset (E-MTAB-863 and E-MTAB-864) (Fig. S1). In this study, high-risk patients were previously defined as those with metastatic cancer recurrence within 5 years of primary surgery (22). We generated differentially expressed gene lists between poor and good prognostic stage II *BRAF*MT CRC tumours (2-fold cut-off; $p < 0.05$) (Fig. S1). IPA analysis, using the significant differential gene list between poor and good prognostic stage II *BRAF*MT CRC, revealed that the UPR was significantly associated with the poor prognostic *BRAF*MT subgroup (Table S3).

GRP78: a key regulator of viability in *BRAF*MT CRC cells. To identify key functional genes/targets for *BRAF*MT CRC, we used an RNAi screening approach targeting proteins that lie at nodal points in the top 20 cancer cell specific pathways identified from the significant up-regulated gene list in poor prognostic stage II/III *BRAF*MT CRC (GSE39582;

Table S1). The effect of down-regulating each of these proteins on cell viability was tested in the *BRAF*MT VACO432, RKO, LIM2405 and HT-29 CRC cells, using an ON-Targetplus siRNA library against 19 targets (Table S4). Notably, only 1/19 siRNAs had a significant inhibitory effect on survival in all 4 *BRAF*MT cell line models, and this was *HSPA5*, the gene encoding the master regulator of UPR, GRP78 (Table S4; Fig. 1A). This was confirmed using additional siRNA sequences against *HSPA5* (Fig. S2A). These results are the first to demonstrate the importance of GRP78 and the UPR as a potential novel target for *BRAF*MT CRC with poor clinical outcome.

GRP78 inhibition induces ER stress and apoptosis in *BRAF*MT CRC cells. Based on the results from the RNAi screen, we next assessed the involvement of GRP78 and the UPR in regulating survival of *BRAF*MT CRC cells. We used a small molecule inhibitor against GRP78, HA15 (15), and the *BRAF*MT VACO432 CRC cell line, and its isogenic VT1 clone with a disrupted $BRAF^{V600E}$ allele (Fig. 1B) (23). A previous study in melanoma has shown that HA15 induces dissociation of GRP78 from PERK, IRE1α and ATF6 complexes. Treatment with HA15 for 24h resulted in phosphorylation of Serine 51 of EIF2α and increases in ATF4 and CHOP, and this was associated with apoptosis induction as indicated by PARP cleavage, caspase-9 cleavage and increased caspase-3/7 activity in the *BRAF*MT VACO432 cell line but *not* in the WT VT1 clone (Fig. 1B, Fig. S2B). Increased phosphorylation of IRE1α on Ser724 and ATF6 cleavage were also observed 48h following treatment with HA15 in the *BRAF*MT cells. Similar results were obtained in the *BRAF*MT HT-29 cell line, but *not* in the *BRAF*WT DiFi, CACO-2 and COLO320 CRC cell line models (Fig. 1C; Fig. S2C, S2D). Treatment with HA15 also resulted in significant reduction in cell viability in the panel of *BRAF*MT CRC cells (Fig. 1C). As expected, treatment of *BRAF*MT cells with the pan-caspase inhibitor Z-VAD-FMK, abolished the effect of HA15 on PARP cleavage; however importantly, caspase inhibition failed to prevent increased IRE1α phosphorylation and induction of ATF4 and CHOP, indicating that ER stress activation is upstream of

apoptosis induction (Fig. S2C). Collectively, these data indicate that GRP78 inhibition induces ER stress and apoptosis in *BRAF*MT CRC.

In order to define the relative importance of the extrinsic and intrinsic apoptotic pathways in mediating HA15-induced apoptosis, we used siRNA specifically directed against caspase-8 (extrinsic pathway) or caspase-9 (intrinsic pathway) (Fig. 1B). Apoptotic cell death (PARP and caspase 3 cleavage) following HA15 treatment was completely abrogated following caspase-8 silencing. In addition, the increased caspase-9 p35/37 cleavage products (indicative of activation of the intrinsic cell death pathway) that were observed following HA15 treatment, were also completely abrogated following caspase-8 silencing. In contrast, caspase-9 silencing resulted only in a partial rescue of the PARP cleavage observed following HA15 treatment. This suggests that the cell death induced by HA15 proceeds via a caspase-8-mediated activation of the caspase-9-dependent intrinsic apoptotic pathway (24). To investigate the mechanism of apoptosis further, we assessed expression levels of pro- and anti-apoptotic proteins following HA15 treatment in the *BRAF*MT VACO432 cell line and its isogenic VT1 clone (Fig. 1C). Notably, expression of the BH3-only proteins NOXA and PUMA, which control the intrinsic cell death pathway, and the death receptor DR5, which activates the extrinsic apoptotic pathway, were markedly up-regulated, whereas expression of anti-apoptotic BCL-2 family members BCL-2 and MCL-1 were downregulated following treatment with HA15 in the *BRAF*MT VACO432 cell line (Fig. 1C). No changes in DR4 expression levels were observed following treatment with HA15 treatment (Fig. S2E). Similar results were obtained in the *BRAF*MT HT-29 cell line. CHOP promotes both the transcription of DR5 (25) and PUMA (26) and the downregulation of BCL-2 expression (27) contributing to the induction of apoptosis. In order to determine whether the ER stress induced by HA15 is responsible for apoptosis, we used siRNA against *DDIT3* (gene encoding CHOP), a gene that mediates ER-stress-induced apoptosis (Fig. 1D). Notably, CHOP silencing abrogated HA15-induced PUMA levels and downregulated MCL-1 levels, and decreased HA15-induced PARP and caspase-3 cleavage in *BRAF*MT CRC cells, indicating that the ER stress-

mediated activation of CHOP is responsible for HA15-induced cell death. Silencing of CHOP also partially reversed the decreased cell viability following HA15 treatment in *BRAF*MT CRC cells (Fig. 1D).

Oncogenic *BRAF* and MEK/ERK trigger increased protein translation, ER stress and sensitivity to the ER stress activator HA15. MEK/ERK pathway activation has been shown to enhance protein translation/synthesis via phosphorylation of the translation initiator eIF4E, thereby exceeding ER protein folding capacity and resulting in ER stress (28). Consistent with this, we found marked increased basal levels of peIF4E^{S209} (Fig. 2A, left) and nascent protein production (Fig. 2A, middle) in the *BRAF*MT VACO432 cell line with activated MEK1/2-ERK1/2 pathway, compared to its WT clone (VT1). In addition, constitutive levels of the ER stress proteins ATF4, CHOP and the active (spliced) form of XBP1 (sXBP1), (indicators of activation of the PERK and IRE1α UPR branches) were also higher in the *BRAF*MT VACO432 cell line, compared to its WT clone (Fig. 2A, right). *DDIT3* and *ATF4* mRNA levels were also higher in the VACO432 cell line compared to the VT1 clone (Fig. 2A, right).

In order to further investigate the relative importance of the BRAF/MEK pathway in regulating sensitivity to the ER stress activator HA15, we used the MEK1/2 inhibitor AZD6244. Treatment of *BRAF*MT cells with AZD6244 potently inhibited peIF4E^{S209} levels (Fig. 2A, left), decreased nascent protein production (Fig. 2B, right) and resulted in a potent reduction in basal ATF4 and CHOP levels (Fig. 2B, left). Importantly, AZD6244 treatment also resulted in a potent downregulation in HA15-induced ATF4 and CHOP levels and this was associated with decreased levels of apoptosis induction following HA15 treatment (Fig. 2C). Similar results were obtained with the MEK1/2 inhibitor trametinib (Fig. S2F and S2G). Moreover, calculation of combination index (CI) values confirmed antagonism between trametinib and HA15 in the *BRAF*MT HT-29 cell line (Fig. S2G). Collectively, these data would suggest that oncogenic *BRAF* and activated MEK1/2-ERK1/2 signalling results in

enhanced protein synthesis and chronic ER stress, rendering *BRAF*MT CRC cells susceptible to apoptosis following treatment with acute ER stress activators such as HA15.

Combination of the ER stress inducers carfilzomib and ACY-1215 results in apoptosis in *BRAF*MT CRC cells. To test our hypothesis that *BRAF*MT CRC cells are vulnerable to modulation of the UPR, we used two inhibitors of protein degradation pathways: the proteasomal inhibitor Carfilzomib (CFZ) (29) and the aggresome inhibitor ACY-1215 (HDAC6-selective inhibitor) (30). These compounds are in clinical development and have been found to result in overload of misfolded/damaged proteins and ER stress. Initially, we evaluated the effects of CFZ and ACY-1215 on viability of the parental *BRAF*MT VACO432 CRC cell line and its isogenic VT1 clone, and a panel of *BRAF*MT (LIM2405, HT-29, COLO205, RKO) and WT (CACO-2, COLO320 and DiFi) CRC cells. Sensitivity to both CFZ and ACY-1215 was markedly higher in the *BRAF*MT VACO432 cell line (5.9nM±2.3 and 1.36μM±0.52 respectively) compared to its WT clone (18.46nM±2.9 and 9.63μM±2.95 respectively), and this was associated with increased apoptosis as determined by PARP cleavage and increased sub-G_1 levels in the VACO432 cells compared to the VT1 cells (Fig. 3A, 3B; Fig. S3A). ACY-1215 caused an increase in acetylation of α-tubulin, a marker of HDAC6 inhibition. There was however no clear pattern of increased sensitivity to CFZ or ACY-1215 in the panel of non-matched *BRAF*MT and WT CRC cells (Fig. S3A).

Next, we investigated the effects of combination treatment of CFZ with ACY-1215 on survival of *BRAF*MT/WT CRC cells. Combined treatment of CFZ with ACY-1215 resulted in potent increases in apoptosis as indicated by increased PARP cleavage and caspase-3 processing, caspase-8 and -3/7 activity assays and flow cytometry in the *BRAF*MT VACO432 cell line but not the WT VT1 clone (Fig. 3B; S3B and S3C). In addition, transient overexpression of *BRAF*V600E led to increased CHOP expression levels and was associated with increased PARP processing and caspase 3/7 activity in response to combined ACY-1215/CFZ treatment in the *BRAF*WT VT1 cells (Fig. 3B). Importantly, similar results were obtained in a

wider panel of *BRAF*MT (HT-29, LIM2405, RKO, COLO205), but *not BRAF*WT CRC cell line models (COLO320, CACO-2, DiFi cells) (Fig. 3C, 3D and S3C). Caspase-dependent apoptosis following CFZ/ACY-1215 treatment was assessed using the pan-caspase inhibitor Z-VAD-FMK, which attenuated apoptosis (Fig. S4A). Silencing of caspase-9 partially reduced PARP and C3 cleavage following CFZ/ACY-1215 co-treatment, suggesting a predominant role of the intrinsic apoptotic pathway in regulating CFZ/ACY-1215-induced cell death (Fig. S4B). Calculation of combination index (CI) values confirmed strong synergy between CFZ and ACY-1215 in all *BRAF*MT CRC cells (Fig. S4C). Taken together, these data would indicate that *BRAF*MT CRC cells show increased sensitivity to dual targeting of protein degradation pathways.

Combination of CFZ and ACY-1215 results in accumulation of misfolded/unfolded proteins and ER stress in *BRAF*MT CRC cells. To investigate the mechanism underlying the observed synergy between CFZ and ACY-1215, we used the PROTEOSTAT® dye, a fluorescent dye that facilitates the detection of aggregated protein cargoes within aggresomes and other inclusion bodies (31). Treatment of the *BRAF*MT VACO432 cells with combined CFZ/ACY-1215 resulted in a marked accumulation of aggregated proteins, compared to the effect of either agent alone (Fig. 4A). Aggregation of proteins following combined CFZ/ACY-1215 treatment was markedly less induced in its *BRAF*WT clone. Moreover, the combination of ACY-1215 with CFZ increased the accumulation of ubiquitinated proteins, in particular in the *BRAF*MT VACO432, COLO205 and RKO cells, but not in the *BRAF*WT VT1 and DiFi cells (Fig. 4B; Fig. S5).

Proteasomal and aggresome inhibition has been shown to induce ER stress (32, 33). In order to explore the role of the UPR in mediating apoptosis following combined CFZ/ACY-1215 treatment, we assessed expression and phosphorylation levels of the pro-apoptotic UPR proteins CHOP and JNK, 24h following treatment with CFZ and ACY-1215 (Fig. 5A, 5B). We found marked increased expression levels of CHOP in all *BRAF*MT but not

*BRAF*WT cells following combined CFZ/ACY-1215 treatment. In addition, increased pJNK$^{T183/Y185}$ was also observed in CFZ/ACY-1215-treated *BRAF*MT HT-29, LIM-2405, RKO and COLO205 cells (Fig. 5A). We also determined the kinetics of activation of the PERK, IRE1α and ATF6 branches of the UPR following co-treatment with CFZ/ACY-1215 and found marked increases in ATF4 and CHOP levels, as early as 6h and 12-24h respectively following co-treatment with CFZ/ACY-1215 in all *BRAF*MT CRC cells (Fig. 5C). Increased IRE1α and JNK activity was observed 6h and 12-24h respectively following treatment with CFZ/ACY-1215, whereas ATF6 cleavage occurred 12-24h following treatment with CFZ/ACY-1215, in particular in the *BRAF*MT COLO205 cells (Fig. 5C).

CHOP is important in regulating CFZ/ACY-1215-induced cell death in *BRAF*MT CRC

To investigate whether activation of the UPR induced by combined CFZ/ACY-1215 treatment is responsible for the observed apoptosis, we used siRNA specifically directed against CHOP. Notably, silencing of CHOP completely abrogated the synergistic induction in caspase-3 and PARP cleavage following combined CFZ/ACY-1215 treatment in *BRAF*MT CRC cells. Collectively, these results would suggest a causal role for the UPR pathway in the cell death following combination of CFZ with ACY-1215 in *BRAF*MT CRC (Fig. 5D).

ACY-1215 in combination with CFZ inhibits the growth of *BRAF*MT xenograft models.

To extend these *in vitro* findings, we next assessed the therapeutic efficacy of combined ACY-1215 and CFZ in the *BRAF*MT VACO432 xenograft model. ACY-1215 and CFZ were administered at 30mg/kg/day IP and Carfilzomib 6mg/kg 3/week IP, the maximum tolerable dose determined in our initial dose escalation study (Fig. S6A). Although both CFZ and ACY-1215 slowed tumour growth, the CFZ/ACY-1215 combination led to a supra-additive reduction in growth in VACO432 *BRAF*MT xenograft model (Fig. 6A, left panel). Furthermore, combined CFZ/ACY-1215 treatment significantly reduced tumour weight, compared to the effect of each treatment alone (Fig. 6A, middle panel). Furthermore, caspase-3 cleavage was observed in the VACO432 tumours following treatment with CFZ in

combination with ACY-1215, indicative of apoptosis induction (Fig. 6A, right panel). The combined treatment was also tolerated in this efficacy study, with only minor weight loss occurring in both vehicle and combination arms (5.96% and 6.1% respectively) (Fig. S6B). These findings indicate that dual targeting of protein degradation pathways using CFZ and ACY-1215 may be highly effective to treat *BRAF*MT CRC.

DISCUSSION

A number of research groups have identified 3-6 molecular subtypes within stage II/III CRC, using gene expression profiles and unsupervised classification (21). Recently, the CRC Subtyping Consortium (CRCSC) has integrated these independent classification systems into 4 Consensus Molecular Subtypes (CMS 1-4) (34). More than 70% of *BRAF*^{V600E} mutant cases were assigned to CMS 1 (with strong association with MSI), whereas 17% and 6% of mutant *BRAF* patients were classified into CMS 4 (cancers which display mesenchymal features with high stromal infiltration) and CMS 3 (cancers with metabolic deregulation) respectively. In order to better characterize the heterogeneity within *BRAF*MT CRC tumours, a recent study performed unsupervised classification of gene expression profiles derived from treated/untreated stage I/II/III *BRAF*MT CRC and identified 2 distinct subgroups: BM1, associated with high KRAS/mTOR/AKT/eEBP1, EMT activation and immune infiltration and BM2 which displays cell-cycle checkpoint dysregulation (35). In this study, we performed for the *first time* supervised clustering of *BRAF*MT gene expression profiles, to identify novel pathways and targets associated with the *BRAF*MT subgroup with poorest outcome. These studies identified a number of biological processes that were deregulated in the *BRAF*MT subgroup with poorest outcome, including the UPR.

Activation of different arms of the UPR have been reported in several solid tumours (36), as well as haematological malignancies (37) and have been identified as a poor prognostic marker in these tumours. In CRC, activation of IRE1α-XBP1 UPR branch has been associated with increased proliferation, invasion and poor prognosis (38). Using a siRNA screening approach and multiple *BRAF*MT cell line models, we identified that GRP78, the master regulator of the UPR, was important for maintaining the viability of *BRAF*MT CRC cells. Moreover, using an inhibitor of GRP78, which dissociates GRP78 from PERK, IRE1α and ATF6 (15), the differential dependency of *BRAF*MT and WT cells on GRP78 for survival was further demonstrated. GRP78 belongs to the heat shock protein 70 (HSP70) family,

facilitates protein folding, targets misfolded proteins for proteasomal degradation and regulates ER stress (39). Overexpression of GRP78 has been observed in many tumours, including CRC (40) and has been associated with resistance to chemotherapy (41). The relative overexpression of GRP78 highlights the potential for exploitation of GRP78 as a therapeutic target in CRC. Increased ERK signalling has been shown to activate protein synthesis, which may result in an imbalance between the ER protein load and folding capacity, resulting in chronic ER stress (42). Indeed, we found that BRAF and MEK regulated levels of eIF4E^{S209}, nascent protein synthesis and ATF4/CHOP and sXBP1 expression levels in *BRAF*MT CRC cells. In contrast to a study from Jiang *et al*. in *BRAF*MT melanoma (43), our study showed that MEK inhibition decreases chronic ER stress and protects *BRAF*MT cells against apoptosis induced by acute ER stress. Furthermore, inhibition of CHOP, a transcription factor that controls the development of programmed cell death in response to acute ER stress (44), prevented apoptosis induced by HA15, indicating the causal role of acute ER stress in HA15-induced apoptosis in *BRAF*MT CRC. These data are the first to show that *BRAF*MT CRC is addicted to the UPR for survival and that UPR activators, such as HA15, result in *acute* ER stress and apoptosis in *BRAF*MT CRC. However, to date there are no existing treatments in routine clinical use that specifically target GRP78.

Proteasome inhibitors (PI) represent a class of agents that exert their anti-cancer effects by inducing accumulation of misfolded poly-ubiquitinated proteins and ER stress (32). There are many PI at various stages of clinical development and, to date, bortezomib, carfilzomib and ixazomib have been approved by the Federal Drugs Administration for use in multiple myeloma (45, 46). In contrast to bortezomib, carfilzomib is an irreversible inhibitor, characterized by a preferential inhibitory potency against the chymotrypsin-like activity of the proteasome, with potent and persistent inhibition (47). Contrary to a previous study in *BRAF*MT CRC (48), we did not find increased sensitivity to carfilzomib across the *BRAF*MT CRC cell line panel, compared to our *BRAF*WT cells. Selective targeting of HDAC6, a class

IIb Histone Deacetylase, results in acetylation of α-tubulin which disrupts binding of the HDAC6-tubulin-dynein motor complex to misfolded protein aggregates and inhibits aggresome-mediated protein degradation, leading to ER stress (33). In addition, a recent study has shown that HDAC6 inhibition results in acetylation of GRP78 and disruption of the GRP78/PERK complex (49). We found that dual targeting of protein degradation pathways, using CFZ and ACY-1215, resulted in marked accumulation of ubiquitinated protein aggregates, caspase-dependent apoptosis and strong synergy in *BRAF*MT CRC cells, but *not BRAF*WT cells. Mechanistically, we found that combined CFZ/ACY-1215 treatment resulted in marked increased expression of pEIF2α^{S51}/ATF4 and pIRE1α^{S724}/pJNK$^{T183/Y185}$, culminating in increased levels of the pro-apoptotic CHOP. Furthermore, we found that siCHOP protected *BRAF*MT CRC from apoptosis following CFZ/ACY-1215 treatment, demonstrating the causal role of the UPR in increased apoptosis following combined CFZ/ACY-1215 treatment in *BRAF*MT CRC. Importantly, we also demonstrated that CFZ in conjunction with ACY-1215 was highly effective at blocking the growth and inducing apoptosis in a *BRAF*MT CRC xenograft.

Combinations of proteasome and HDAC inhibitors have been translated into clinical trials on the basis of dual inhibition of the aggresome and proteasome pathway, in particular in haematological disease. The VANTAGE 095 phase IIb trial of vorinostat (MK-0683) and bortezomib showed a signal of activity in patients with relapsed/refractory multiple myeloma (50). More recent studies using the selective HDAC6 inhibitor ACY-1215 and bortezomib or the more potent proteasome inhibitor CFZ have shown strong synergy in preclinical models of lymphoma and multiple myeloma respectively (49, 51). This is the first study showing that dual aggresome/proteasome inhibition could be a promising treatment strategy for *BRAF*MT CRC patients. This study does not exclude that other poor prognostic subtypes eg. subgroups of *BRAF*WT/*RAS*MT CRC may also be associated with chronic ER stress and therefore could potentially benefit from acute ER stress inducers.

In conclusion, using a systems biology approach, we have identified the UPR as an important, novel and druggable target for the *BRAF*MT CRC subgroup with poorest clinical outcome. We have shown that *BRAF*MT CRC induces *chronic* ER stress, is addicted to the UPR for survival and that UPR activators result in *acute* ER stress and apoptosis in *BRAF*MT CRC (Fig. 6B). From a clinical perspective, the substantial tumour growth inhibition observed in our xenograft study support the evaluation of UPR activators (eg. aggresome/proteasome co-inhibition or more specific ATF4/CHOP activators (52)) in clinical trials for patients with metastatic *BRAF*MT CRC.

ACKNOWLEDGMENTS

We thank Enzo Medico, Andrea Bertotti and Dan Longley for providing bioinformatic and *in vivo* support respectively.

REFERENCES

1. Pakneshan S, Salajegheh A, Smith RA, Lam AK. Clinicopathological relevance of BRAF mutations in human cancer. Pathology. 2013;45:346-56.
2. Popovici V, Budinska E, Tejpar S, Weinrich S, Estrella H, Hodgson G, et al. Identification of a poor-prognosis BRAF-mutant-like population of patients with colon cancer. J Clin Oncol. 2012;30:1288-95.
3. Kopetz S, Desai J, Chan E, Hecht JR, O'Dwyer PJ, Lee RJ, et al. PLX4032 in metastatic colorectal cancer patients with mutant BRAF tumors. J Clin Oncol 2010;28: 15s (suppl; abstr 3534).
4. Yaeger R, Cercek A, O'Reilly EM, Reidy DL, Kemeny N, Wolinsky T, et al. Pilot trial of combined BRAF and EGFR inhibition in BRAF-mutant metastatic colorectal cancer patients. Clin Cancer Res. 2015;21:1313-20.
5. Atreya CE, Van Cutsem E, Bendell JC, Andre T, Schellens JH, Gordon MS, et al. Updated efficacy of the MEK inhibitor trametinib (T), BRAF inhibitor dabrafenib (D), and anti-EGFR antibody panitumumab (P) in patients (pts) with BRAF V600E mutated (BRAFm) metastatic colorectal cancer (mCRC). J Clin Oncol 33, 2015 (suppl; abstr 103).
6. Schwarz DS, Blower MD. The endoplasmic reticulum: structure, function and response to cellular signaling. Cell Mol Life Sci. 2016;73:79-94.
7. Harding HP, Zhang Y, Bertolotti A, Zeng H, Ron D. Perk is essential for translational regulation and cell survival during the unfolded protein response. Molecular cell. 2000;5:897-904.
8. Liu CY, Xu Z, Kaufman RJ. Structure and intermolecular interactions of the luminal dimerization domain of human IRE1alpha. J Biol Chem. 2003;278:17680-7.
9. Shen J, Chen X, Hendershot L, Prywes R. ER stress regulation of ATF6 localization by dissociation of BiP/GRP78 binding and unmasking of Golgi localization signals. Developmental cell. 2002;3:99-111.
10. Tabas I, Ron D. Integrating the mechanisms of apoptosis induced by endoplasmic reticulum stress. Nat Cell Biol. 2011;13:184-90.
11. Puthalakath H, O'Reilly LA, Gunn P, Lee L, Kelly PN, Huntington ND, et al. ER stress triggers apoptosis by activating BH3-only protein Bim. Cell. 2007;129:1337-49.
12. Yamaguchi H, Wang HG. CHOP is involved in endoplasmic reticulum stress-induced apoptosis by enhancing DR5 expression in human carcinoma cells. J Biol Chem. 2004;279:45495-502.
13. Yeh TC, Marsh V, Bernat BA, Ballard J, Colwell H, Evans RJ, et al. Biological characterization of ARRY-142886 (AZD6244), a potent, highly selective mitogen-activated protein kinase kinase 1/2 inhibitor. Clin Cancer Res. 2007;13:1576-83.
14. Berger AB, Witte MD, Denault JB, Sadaghiani AM, Sexton KM, Salvesen GS, et al. Identification of early intermediates of caspase activation using selective inhibitors and activity-based probes. Molecular cell. 2006;23:509-21.
15. Cerezo M, Lehraiki A, Millet A, Rouaud F, Plaisant M, Jaune E, et al. Compounds Triggering ER Stress Exert Anti-Melanoma Effects and Overcome BRAF Inhibitor Resistance. Cancer Cell. 2016;29:805-19.
16. Marais R, Light Y, Paterson HF, Mason CS, Marshall CJ. Differential regulation of Raf-1, A-Raf, and B-Raf by oncogenic ras and tyrosine kinases. J Biol Chem. 1997;272:4378-83.
17. Van Schaeybroeck S, Kyula JN, Fenton A, Fenning CS, Sasazuki T, Shirasawa S, et al. Oncogenic Kras promotes chemotherapy-induced growth factor shedding via ADAM17. Cancer Res. 2011;71:1071-80.
18. Van Schaeybroeck S, Kalimutho M, Dunne PD, Carson R, Allen W, Jithesh PV, et al. ADAM17-dependent c-MET-STAT3 signaling mediates resistance to MEK inhibitors in KRAS mutant colorectal cancer. Cell reports. 2014;7:1940-55.

19. Whitehead RH, Zhang HH, Hayward IP. Retention of tissue-specific phenotype in a panel of colon carcinoma cell lines: relationship to clinical correlates. Immunol Cell Biol. 1992;70 (Pt 4):227-36.
20. Montagut C, Dalmases A, Bellosillo B, Crespo M, Pairet S, Iglesias M, et al. Identification of a mutation in the extracellular domain of the Epidermal Growth Factor Receptor conferring cetuximab resistance in colorectal cancer. Nat Med. 2012;18:221-3.
21. Marisa L, de Reynies A, Duval A, Selves J, Gaub MP, Vescovo L, et al. Gene expression classification of colon cancer into molecular subtypes: characterization, validation, and prognostic value. PLoS medicine. 2013;10:e1001453.
22. Kennedy RD, Bylesjo M, Kerr P, Davison T, Black JM, Kay EW, et al. Development and Independent Validation of a Prognostic Assay for Stage II Colon Cancer Using Formalin-Fixed Paraffin-Embedded Tissue. J Clin Oncol. 2011; 29:4620-6.
23. Yun J, Rago C, Cheong I, Pagliarini R, Angenendt P, Rajagopalan H, et al. Glucose deprivation contributes to the development of KRAS pathway mutations in tumor cells. Science. 2009;325:1555-9.
24. Li H, Zhu H, Xu CJ, Yuan J. Cleavage of BID by caspase 8 mediates the mitochondrial damage in the Fas pathway of apoptosis. Cell. 1998;94:491-501.
25. Lu M, Lawrence DA, Marsters S, Acosta-Alvear D, Kimmig P, Mendez AS, et al. Opposing unfolded-protein-response signals converge on death receptor 5 to control apoptosis. Science. 2014;345:98-101.
26. Cazanave SC, Elmi NA, Akazawa Y, Bronk SF, Mott JL, Gores GJ. CHOP and AP-1 cooperatively mediate PUMA expression during lipoapoptosis. Am J Physiol Gastrointest Liver Physiol. 2010;299:G236-43.
27. McCullough KD, Martindale JL, Klotz LO, Aw TY, Holbrook NJ. Gadd153 sensitizes cells to endoplasmic reticulum stress by down-regulating Bcl2 and perturbing the cellular redox state. Molecular and cellular biology. 2001;21:1249-59.
28. Hou J, Lam F, Proud C, Wang S. Targeting Mnks for cancer therapy. Oncotarget. 2012;3:118-31.
29. Kortuem KM, Stewart AK. Carfilzomib. Blood. 2013;121:893-7.
30. Santo L, Hideshima T, Kung AL, Tseng JC, Tamang D, Yang M, et al. Preclinical activity, pharmacodynamic, and pharmacokinetic properties of a selective HDAC6 inhibitor, ACY-1215, in combination with bortezomib in multiple myeloma. Blood. 2012;119:2579-89.
31. Shen D, Coleman J, Chan E, Nicholson TP, Dai L, Sheppard PW, et al. Novel cell- and tissue-based assays for detecting misfolded and aggregated protein accumulation within aggresomes and inclusion bodies. Cell Biochem Biophys. 2011;60:173-85.
32. Obeng EA, Carlson LM, Gutman DM, Harrington WJ, Jr., Lee KP, Boise LH. Proteasome inhibitors induce a terminal unfolded protein response in multiple myeloma cells. Blood. 2006;107:4907-16.
33. Kawaguchi Y, Kovacs JJ, McLaurin A, Vance JM, Ito A, Yao TP. The deacetylase HDAC6 regulates aggresome formation and cell viability in response to misfolded protein stress. Cell. 2003;115:727-38.
34. Guinney J, Dienstmann R, Wang X, de Reynies A, Schlicker A, Soneson C, et al. The consensus molecular subtypes of colorectal cancer. Nat Med. 2015;21:1350-6.
35. Barras D, Missiaglia E, Wirapati P, Sieber OM, Jorissen RN, Love C, et al. BRAF V600E Mutant Colorectal Cancer Subtypes Based on Gene Expression. Clin Cancer Res. 2017;23:104-15.
36. Penaranda Fajardo NM, Meijer C, Kruyt FA. The endoplasmic reticulum stress/unfolded protein response in gliomagenesis, tumor progression and as a therapeutic target in glioblastoma. Biochemical pharmacology. 2016;118:1-8.
37. Chen L, Li Q, She T, Li H, Yue Y, Gao S, et al. IRE1alpha-XBP1 signaling pathway, a potential therapeutic target in multiple myeloma. Leuk Res. 2016;49:7-12.

38. Jin C, Jin Z, Chen NZ, Lu M, Liu CB, Hu WL, et al. Activation of IRE1alpha-XBP1 pathway induces cell proliferation and invasion in colorectal carcinoma. Biochem Biophys Res Commun. 2016;470:75-81.
39. Lee AS. GRP78 induction in cancer: therapeutic and prognostic implications. Cancer Res. 2007;67:3496-9.
40. Piton N, Wason J, Colasse E, Cornic M, Lemoine F, Le Pessot F, et al. Endoplasmic reticulum stress, unfolded protein response and development of colon adenocarcinoma. Virchows Arch. 2016;469:145-54.
41. Mhaidat NM, Alzoubi KH, Almomani N, Khabour OF. Expression of glucose regulated protein 78 (GRP78) determines colorectal cancer response to chemotherapy. Cancer Biomark. 2015;15:197-203.
42. Oslowski CM, Urano F. Measuring ER stress and the unfolded protein response using mammalian tissue culture system. Methods Enzymol. 2011;490:71-92.
43. Jiang CC, Chen LH, Gillespie S, Wang YF, Kiejda KA, Zhang XD, et al. Inhibition of MEK sensitizes human melanoma cells to endoplasmic reticulum stress-induced apoptosis. Cancer Res. 2007;67:9750-61.
44. Zinszner H, Kuroda M, Wang X, Batchvarova N, Lightfoot RT, Remotti H, et al. CHOP is implicated in programmed cell death in response to impaired function of the endoplasmic reticulum. Genes & development. 1998;12:982-95.
45. Teicher BA, Tomaszewski JE. Proteasome inhibitors. Biochemical pharmacology. 2015;96:1-9.
46. Shirley M. Ixazomib: First Global Approval. Drugs. 2016;76:405-11.
47. Kuhn DJ, Chen Q, Voorhees PM, Strader JS, Shenk KD, Sun CM, et al. Potent activity of carfilzomib, a novel, irreversible inhibitor of the ubiquitin-proteasome pathway, against preclinical models of multiple myeloma. Blood. 2007;110:3281-90.
48. Zecchin D, Boscaro V, Medico E, Barault L, Martini M, Arena S, et al. BRAF V600E is a determinant of sensitivity to proteasome inhibitors. Mol Cancer Ther. 2013;12:2950-61.
49. Amengual JE, Johannet P, Lombardo M, Zullo K, Hoehn D, Bhagat G, et al. Dual Targeting of Protein Degradation Pathways with the Selective HDAC6 Inhibitor ACY-1215 and Bortezomib Is Synergistic in Lymphoma. Clin Cancer Res. 2015;21:4663-75.
50. Siegel DS, Dimopoulos M, Jagannath S, Goldschmidt H, Durrant S, Kaufman JL, et al. VANTAGE 095: An International, Multicenter, Open-Label Study of Vorinostat (MK-0683) in Combination With Bortezomib in Patients With Relapsed and Refractory Multiple Myeloma. Clin Lymphoma Myeloma Leuk. 2016;16:329-34 e1.
51. Mishima Y, Santo L, Eda H, Cirstea D, Nemani N, Yee AJ, et al. Ricolinostat (ACY-1215) induced inhibition of aggresome formation accelerates carfilzomib-induced multiple myeloma cell death. British journal of haematology. 2015;169:423-34.
52. Allen JE, Kline CL, Prabhu VV, Wagner J, Ishizawa J, Madhukar N, et al. Discovery and clinical introduction of first-in-class imipridone ONC201. Oncotarget. 2016;7:74380-92.

FIGURE LEGENDS

Figure 1. *BRAF*MT CRC cells are dependent on the UPR for survival. A. Results of the siRNA screen. *BRAF*MT cells were reverse transfected with all stars' non-targeted siRNA sequence and sequence specific siRNA. Cell viability was calculated following 72h transfection using the CellTitre-Glo™ assay. Data for siHSPA5 are shown. Western blotting (WB) for GRP78 and PARP following siHSPA5 (HA) for 48h. Full siRNA screen data can be found in Table S4. **B. Left:** PARP, pEIF2α^{S51}, EIF2α, ATF4, CHOP, ATF6, GRP78, pIRE1α^{S724} and IRE1α expression in VACO432 and VT1 cells, following treatment with HA15 for the indicated time. **Right upper:** Caspase-3/7 activity levels in VACO432 cells, following treatment with HA15. **Right lower**: VACO432 cells were transfected with scrambled control (SC), caspase-8 (siC8) or caspase-9 siRNA (siC9) for 24h and thereafter treated with HA15 for 24h. Cleaved-PARP, caspase-3, pro-caspase-8 and caspase-9 were determined by WB. **C. Upper:** PARP, BCL-2, BCL-XL, MCL-1, PUMA, NOXA, BID and BIM levels in *BRAF*MT VACO432, HT-29 and *BRAF*WT VT1 cells following treatment with HA15 for the indicated time. **Lower left**: CRC cells were treated with HA15 for 24h and DR5 cell membrane expression assessed by flow cytometry using receptor-specific phycoerythrin-conjugated mAbs. Expression was compared with a nonspecific isotype-matched control antibody. **Lower right:** MTT cell viability of *BRAF*MT cells following 72h treatment with HA15. **D. Upper:** VACO432 cells were transfected with SC or DDIT3 (siCH) siRNA for 24h and thereafter treated with HA15 for 24h. Cleaved-PARP, caspase-3, CHOP, PUMA, BCL-2 and MCL-1 expression were determined by WB. **Lower:** MTT cell viability of *BRAF*MT cells transfected with siCH and co-treated with HA15 for 72h. SE=short exposure; LE=long exposure.

Figure 2. MEK/ERK trigger sensitivity to the ER stress activator HA15. A. Left: *BRAF*MT VACO432 and LIM2405 and *BRAF*WT VT1 cells were treated with AZD6244 for 24h and peIF4E^{S209}, eIF4E, pERK1/2, ERK1/2, pMEK1/2 and MEK1/2 levels determined by WB. **Middle:** Representative image of Click-iT protein synthesis assay in VACO432 and VT1

cells. **Right:** BRAF, ERK1/2, pERK1/2, ATF4, CHOP and sXBP1 basal expression in VACO432 and VT1 cells determined by WB and/or real-time PCR. **B. Left:** ATF4, CHOP, sXBP1, GRP78 and ERK1/2 expression following 24h treatment with AZD6244 in *BRAF*MT cells. **Right:** Representative image of Click-iT protein synthesis assay in VACO432 cells following treatment with AZD6244 for 24h. **C.** PARP, ATF4, CHOP, sXBP1, GRP78 and ERK1/2 levels following co-treatment with AZD6244 and HA15 for 24h. Scale bar represents 20 micrometer. SE=short exposure; LE=long exposure.

Figure 3. Dual targeting of the aggresome and proteasome pathway results in cell death in *BRAF*MT CRC. A. WB analysis of PARP and acetylated-*α*-tubulin in CRC cells following treatment with ACY-1215 or Carfilzomib (CFZ) for 24h. **B**. **Left upper:** CRC cells were co-treated with ACY-1215 and CFZ for 24h and PARP, cleaved caspase-8 (C8), cleaved caspase-3 (C3) and acetylated-*α*-tubulin determined by WB. **Left lower:** Annexin V/PI flow cytometric analysis of CRC cells following treatment with ACY-1215 and CFZ for 24h. **Right:** Expression of BRAF, pMEK1/2, MEK1/2, pERK1/2, ERK1/2, CHOP and PARP (**upper**) and C3/7 activity levels (**lower**) in VT1 cells transiently transfected with 1µg of *BRAF*V600E expression construct for 12h followed by 24h treatment with ACY-1215, CFZ or ACY-1215/CFZ. **C.** *BRAF*MT cells were co-treated with ACY-1215 and CFZ for 24h and apoptosis determined by WB for PARP, cleaved-C8 and cleaved-C3 (**upper**) and PI flow cytometry (**lower**). **D.** *BRAF/KRAS*WT COLO320, CACO-2 and DiFi cells were treated with ACY-1215 and Carfilzomib for 24h and PARP, cleaved caspase 8 (p43/41), cleaved caspase 3, and acetylated α tubulin expression levels determined by WB. *BRAF*MT VACO432 cells were treated with ACY-1215/CFZ for 24h.

Figure 4. Combined aggresome/proteasome inhibition results in accumulation of aggregated proteins in *BRAF*MT CRC cells. A. Protein aggregates in CRC cells, treated with ACY-1215, CFZ or combination (Proteostat™ dye (red), counterstained with Hoechst

33342). Scale bar represents 20 micrometer. **B.** Total levels of ubiquitinated proteins in *BRAF*MT/WT CRC cells, treated with ACY-1215 and CFZ for 12h.

Figure 5. Dual targeting of protein degradation pathways results in acute ER stress and apoptosis. A. CRC cells were treated with CFZ alone or combined with ACY-1215 and PARP, CHOP, pJNK$^{T183/Y185}$ and JNK levels determined by WB. **B.** CRC cells were treated with CFZ alone or combined with ACY-1215 for 24h and *DDIT3* mRNA levels determined by real-time PCR. Relative mRNA expression was calculated using the DDCt method with normalisation to β-actin and GAPDH. **C.** PARP and levels of UPR proteins in *BRAF*MT cells following treatment with ACY-1215 and/or CFZ for the indicated times. **D.** LIM2405 cells were transfected with SC or siCH for 24h and thereafter treated with ACY-1215 and CFZ for 24h. PARP, cleaved-C3 and CHOP expression were determined by WB and/or activity assay.

Figure 6. Combined ACY-1215/CFZ treatment results in reduction in growth of *BRAF*MT CRC *in vivo*. A. Growth rate (**left**) and tumour weights at day 15 (**middle**) of VACO432 xenografts in BALB/c Nude mice treated with vehicle, ACY-1215, CFZ or in combination. Differences in growth were determined using Student's t-test. WB analysis for cleaved-C3 in tumour samples **(Right)**. **B.** Schematic overview of proposed model. As a result of enhanced protein synthesis, *BRAF*MT CRC tumours induce *chronic* ER stress, resulting in cancer cell survival. ACY-1215/CFZ and HA15 result in *acute* ER stress, increased CHOP expression and apoptosis, through activation of both extrinsic and extrinsic cell death pathways.

Figure 1

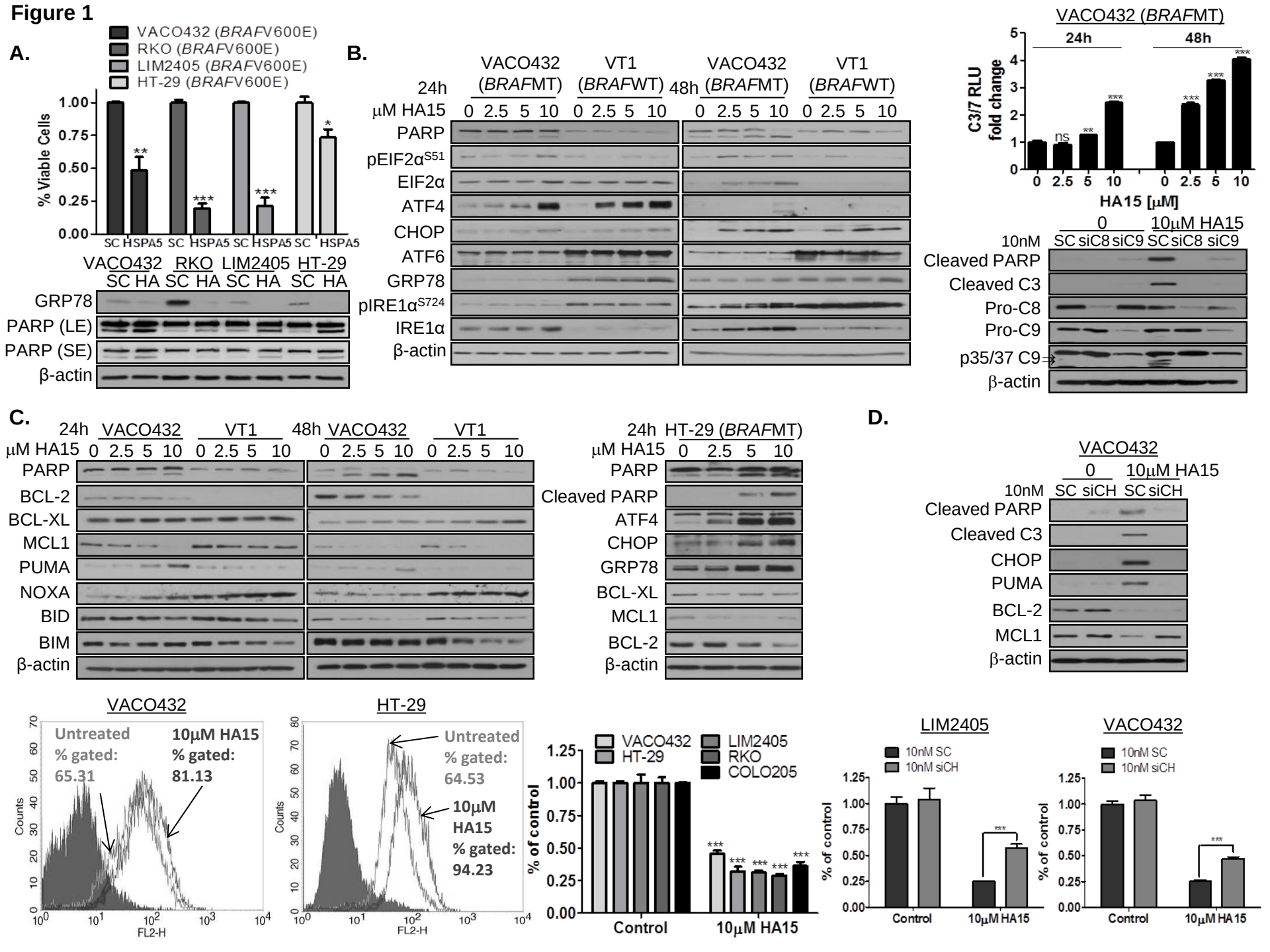
A.
VACO432 (BRAFV600E)
RKO (BRAFV600E)
LIM2405 (BRAFV600E)
HT-29 (BRAFV600E)
% Viable Cells
SC HSPA5 SC HSPA5 SC HSPA5 SC HSPA5
VACO432 RKO LIM2405 HT-29
SC HA SC HA SC HA SC HA
GRP78
PARP (LE)
PARP (SE)
β-actin
B.
24h 48h
VACO432 (BRAFMT) VT1 (BRAFWT) VACO432 (BRAFMT) VT1 (BRAFWT)
μM HA15 0 2.5 5 10 0 2.5 5 10 0 2.5 5 10 0 2.5 5 10
PARP
pEIF2αS51
EIF2α
ATF4
CHOP
ATF6
GRP78
pIRE1αS724
IRE1α
β-actin
VACO432 (BRAFMT)
24h 48h
C3/7 RLU fold change
ns
HA15 [μM]
0 10μM HA15
10nM SC siC8 siC9 SC siC8 siC9
Cleaved PARP
Cleaved C3
Pro-C8
Pro-C9
p35/37 C9
β-actin
C.
24h VACO432 VT1 48h VACO432 VT1
μM HA15 0 2.5 5 10 0 2.5 5 10 0 2.5 5 10 0 2.5 5 10
PARP
BCL-2
BCL-XL
MCL1
PUMA
NOXA
BID
BIM
β-actin
24h HT-29 (BRAFMT)
μM HA15 0 2.5 5 10
PARP
Cleaved PARP
ATF4
CHOP
GRP78
BCL-XL
MCL1
BCL-2
β-actin
D.
VACO432
0 10μM HA15
10nM SC siCH SC siCH
Cleaved PARP
Cleaved C3
CHOP
PUMA
BCL-2
MCL1
β-actin
VACO432
Untreated
% gated:
65.31
10μM HA15
% gated:
81.13
Counts
FL2-H
HT-29
Untreated
% gated:
64.53
10μM HA15
% gated:
94.23
VACO432
HT-29
LIM2405
RKO
COLO205
% of control
Control
10μM HA15
LIM2405
10nM SC
10nM siCH
VACO432
10nM SC
10nM siCH

Figure 2

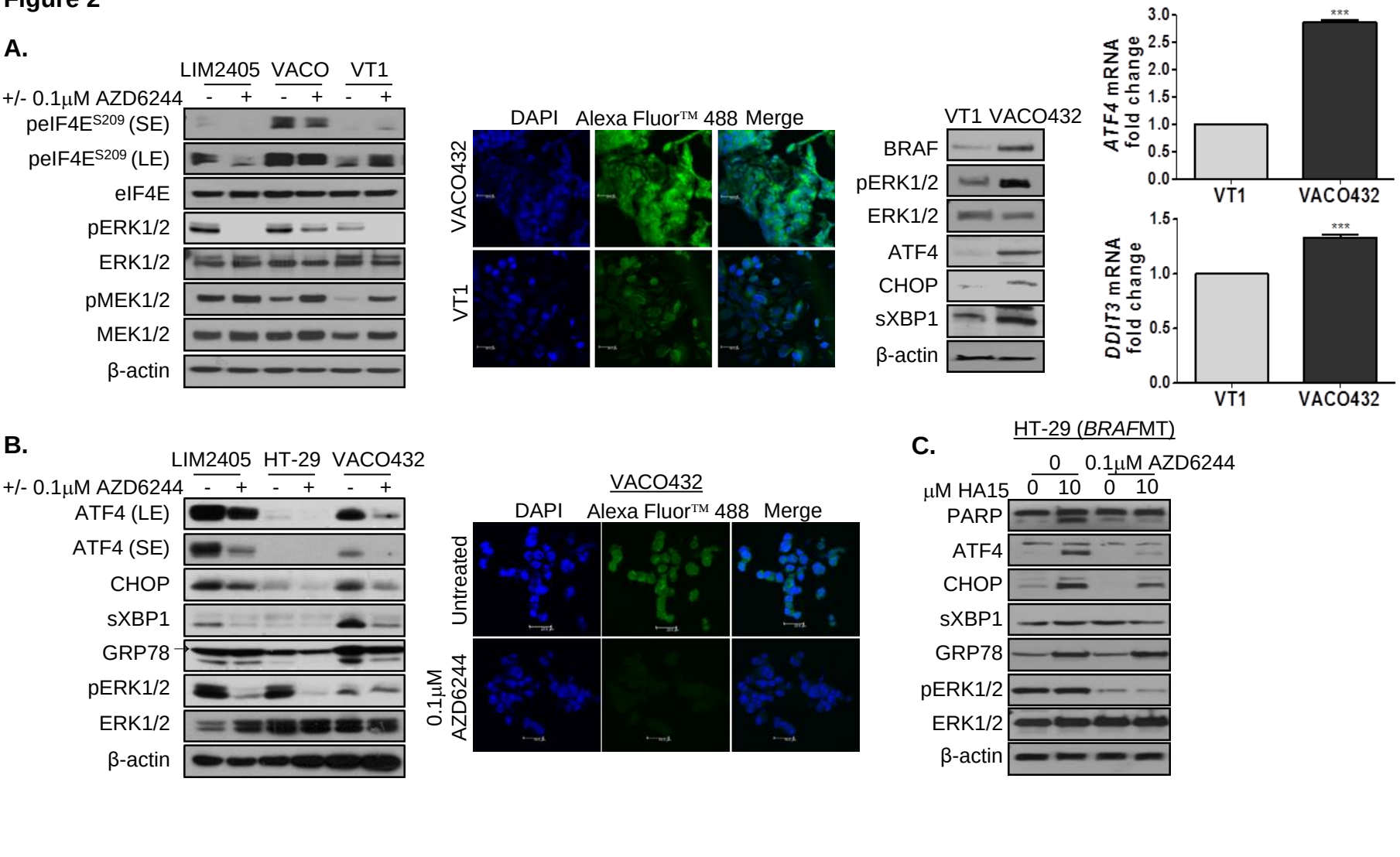
A.
LIM2405 VACO VT1
+/- 0.1μM AZD6244 - + - + - +
peIF4E^S209 (SE)
peIF4E^S209 (LE)
eIF4E
pERK1/2
ERK1/2
pMEK1/2
MEK1/2
β-actin
DAPI Alexa Fluor™ 488 Merge
VACO432
VT1
VT1 VACO432
BRAF
pERK1/2
ERK1/2
ATF4
CHOP
sXBP1
β-actin
ATF4 mRNA fold change
DDIT3 mRNA fold change
VT1
VACO432
***
B.
LIM2405 HT-29 VACO432
+/- 0.1μM AZD6244 - + - + - +
ATF4 (LE)
ATF4 (SE)
CHOP
sXBP1
GRP78
pERK1/2
ERK1/2
β-actin
VACO432
DAPI Alexa Fluor™ 488 Merge
Untreated
0.1μM AZD6244
C.
HT-29 (BRAFMT)
0 0.1μM AZD6244
μM HA15 0 10 0 10
PARP
ATF4
CHOP
sXBP1
GRP78
pERK1/2
ERK1/2
β-actin

Figure 3

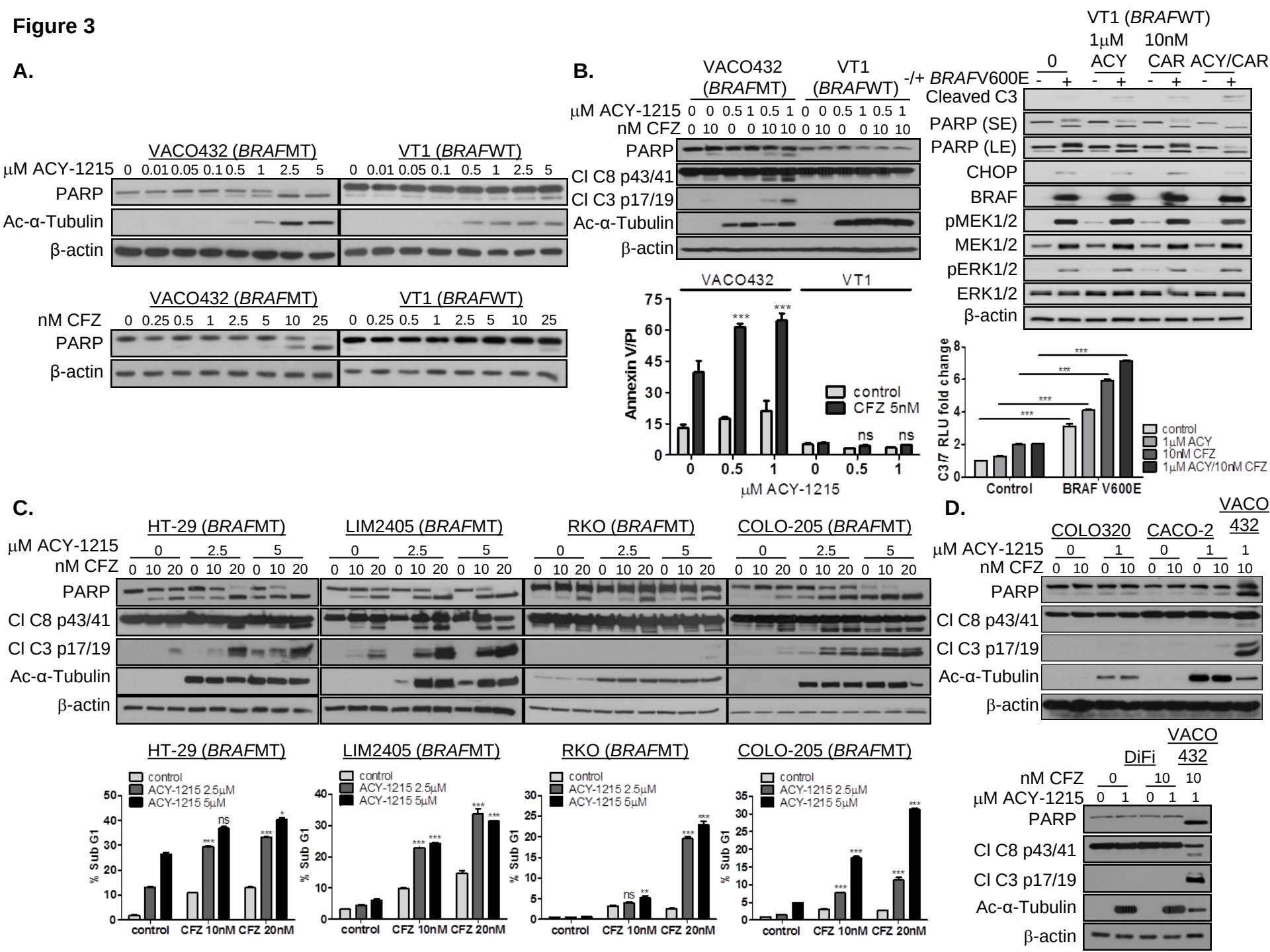
A.
VACO432 (BRAFMT)
VT1 (BRAFWT)
μM ACY-1215 0 0.01 0.05 0.1 0.5 1 2.5 5
PARP
Ac-α-Tubulin
β-actin
nM CFZ 0 0.25 0.5 1 2.5 5 10 25
B.
VACO432 (BRAFMT)
VT1 (BRAFWT)
μM ACY-1215 0 0 0.5 1 0.5 1 0 0 0.5 1 0.5 1
nM CFZ 0 10 0 0 10 10 0 10 0 0 10 10
Cl C8 p43/41
Cl C3 p17/19
Annexin V/PI
control
CFZ 5nM
ns
μM ACY-1215
VT1 (BRAFWT)
-/+ BRAFV600E
0
1μM ACY
10nM CAR
ACY/CAR
Cleaved C3
PARP (SE)
PARP (LE)
CHOP
BRAF
pMEK1/2
MEK1/2
pERK1/2
ERK1/2
C3/7 RLU fold change
control
1μM ACY
10nM CFZ
1μM ACY/10nM CFZ
Control
BRAF V600E
C.
HT-29 (BRAFMT)
LIM2405 (BRAFMT)
RKO (BRAFMT)
COLO-205 (BRAFMT)
μM ACY-1215
nM CFZ
PARP
Cl C8 p43/41
Cl C3 p17/19
Ac-α-Tubulin
β-actin
% Sub G1
control
ACY-1215 2.5μM
ACY-1215 5μM
CFZ 10nM
CFZ 20nM
D.
VACO 432
COLO320
CACO-2
DiFi
nM CFZ
μM ACY-1215
PARP
Cl C8 p43/41
Cl C3 p17/19
Ac-α-Tubulin
β-actin

Figure 4

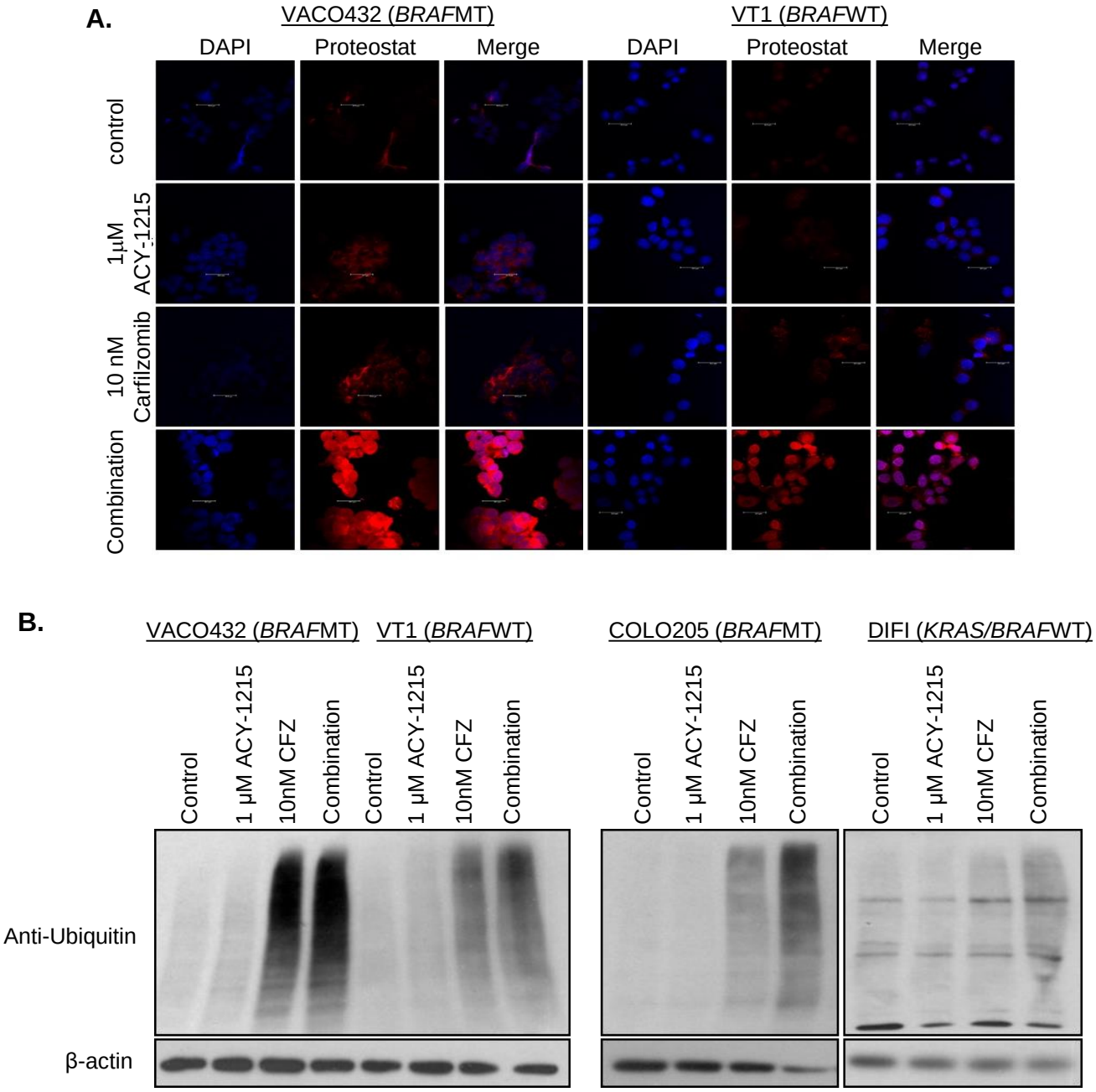
A.
VACO432 (BRAFMT)
VT1 (BRAFWT)
DAPI
Proteostat
Merge
DAPI
Proteostat
Merge
control
1μM ACY-1215
10 nM Carfilzomib
Combination
B.
VACO432 (BRAFMT)
VT1 (BRAFWT)
COLO205 (BRAFMT)
DIFI (KRAS/BRAFWT)
Control
1 μM ACY-1215
10nM CFZ
Combination
Anti-Ubiquitin
β-actin

Figure 5

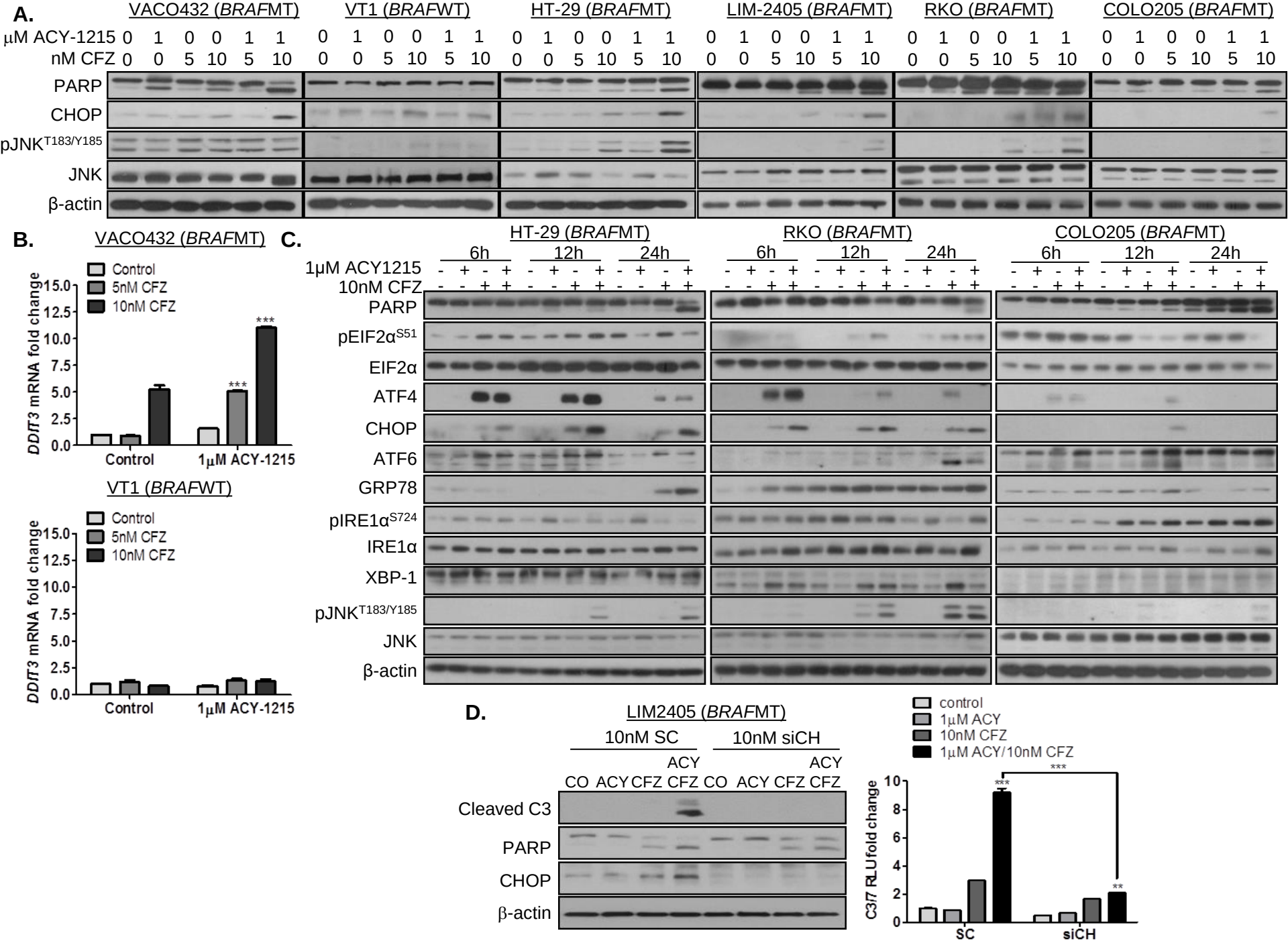
A.
VACO432 (BRAFMT)
VT1 (BRAFWT)
HT-29 (BRAFMT)
LIM-2405 (BRAFMT)
RKO (BRAFMT)
COLO205 (BRAFMT)
μM ACY-1215
nM CFZ
PARP
CHOP
pJNKT183/Y185
JNK
β-actin
B.
VACO432 (BRAFMT)
Control
5nM CFZ
10nM CFZ
DDIT3 mRNA fold change
Control
1μM ACY-1215
VT1 (BRAFWT)
C.
HT-29 (BRAFMT)
RKO (BRAFMT)
COLO205 (BRAFMT)
6h
12h
24h
1μM ACY1215
10nM CFZ
PARP
pEIF2αS51
EIF2α
ATF4
CHOP
ATF6
GRP78
pIRE1αS724
IRE1α
XBP-1
pJNKT183/Y185
JNK
β-actin
D.
LIM2405 (BRAFMT)
10nM SC
10nM siCH
ACY
CO ACY CFZ CFZ CO ACY CFZ CFZ
Cleaved C3
PARP
CHOP
β-actin
control
1μM ACY
10nM CFZ
1μM ACY/10nM CFZ
C3/7 RLU fold change
SC
siCH

Figure 6

A.

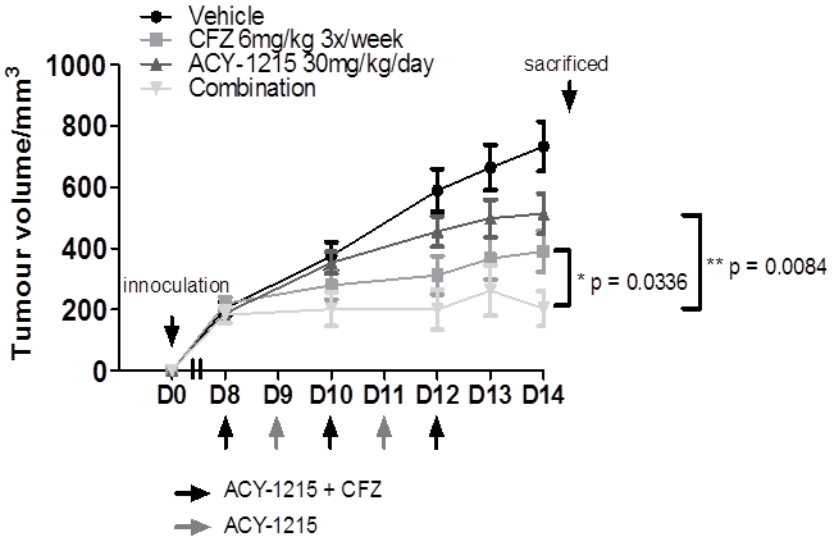
Vehicle
CFZ 6mg/kg 3x/week
ACY-1215 30mg/kg/day
Combination
sacrificed
Tumour volume/mm3
1000
800
600
400
200
0
innoculation
* p = 0.0336
** p = 0.0084
D0 D8 D9 D10 D11 D12 D13 D14
ACY-1215 + CFZ
ACY-1215

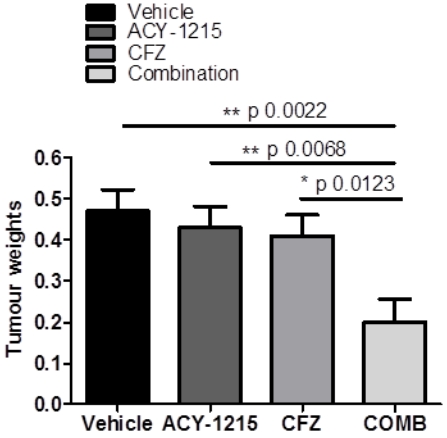
Vehicle
ACY-1215
CFZ
Combination
** p 0.0022
** p 0.0068
* p 0.0123
Tumour weights
0.6
0.5
0.4
0.3
0.2
0.1
0.0
Vehicle ACY-1215 CFZ COMB

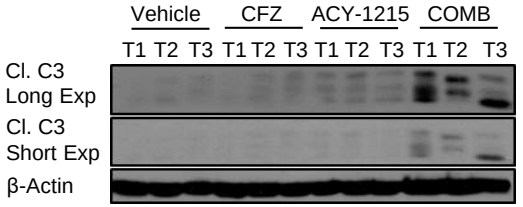
Vehicle
CFZ
ACY-1215
COMB
T1 T2 T3 T1 T2 T3 T1 T2 T3 T1 T2 T3
Cl. C3
Long Exp
Cl. C3
Short Exp
β-Actin

B.

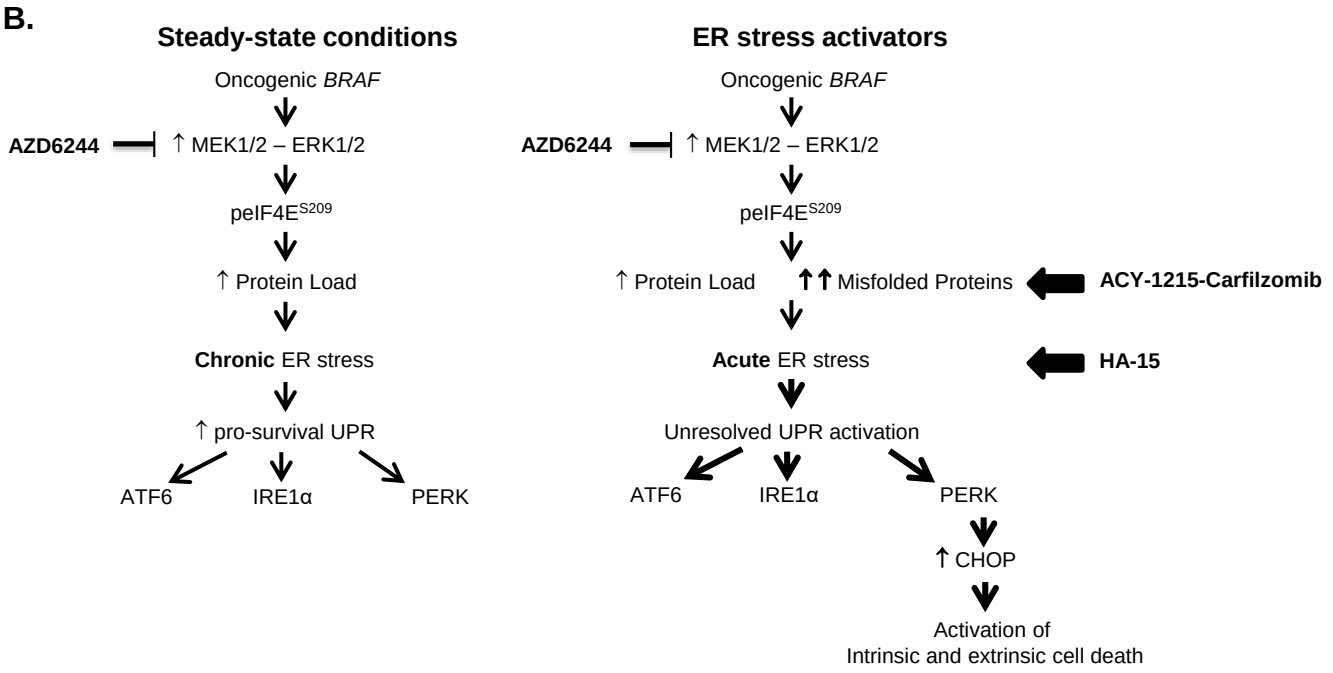
Steady-state conditions
Oncogenic BRAF
AZD6244
↑ MEK1/2 – ERK1/2
peIF4E S209
↑ Protein Load
Chronic ER stress
↑ pro-survival UPR
ATF6
IRE1α
PERK
ER stress activators
Oncogenic BRAF
AZD6244
↑ MEK1/2 – ERK1/2
peIF4E S209
↑ Protein Load
↑↑ Misfolded Proteins
ACY-1215-Carfilzomib
Acute ER stress
HA-15
Unresolved UPR activation
ATF6
IRE1α
PERK
↑ CHOP
Activation of
Intrinsic and extrinsic cell death